

Article

On the Symmetry, Electronic Properties, and Possible Metallic States in NASICON-Structured $A_4V_2(PO_4)_3$ (A = Li, Na, K) Phosphates

Denis Gryaznov ^{1,2,*}  and Linas Vilčiauskas ^{1,*} ¹ Center for Physical Sciences and Technology (FTMC), Saulėtekio al. 3, LT-10257 Vilnius, Lithuania² Institute of Solid State Physics, University of Latvia, Kengaraga 8, LV-1063 Riga, Latvia

* Correspondence: gryaznov@mail.com (D.G.); linas.vilciauskas@ftmc.lt (L.V.)

Abstract: In this work, the electronic structure and properties of NASICON-structured $A_4V_2(PO_4)_3$, where A = Li, Na, K were studied using hybrid density functional theory calculations. The symmetries were analyzed using a group theoretical approach, and the band structures were examined by the atom and orbital projected density of states analyses. $Li_4V_2(PO_4)_3$ and $Na_4V_2(PO_4)_3$ adopted monoclinic structures with the C2 space group and averaged vanadium oxidation states of $V^{+2.5}$ in the ground state, whereas $K_4V_2(PO_4)_3$ adopted a monoclinic structure with the C2 space group and mixed vanadium oxidation states V^{+2}/V^{+3} in the ground state. The mixed oxidation state is the least stable state in $Na_4V_2(PO_4)_3$ and $Li_4V_2(PO_4)_3$. Symmetry increases in $Li_4V_2(PO_4)_3$ and $Na_4V_2(PO_4)_3$ led to the appearance of a metallic state that was independent of the vanadium oxidation states (except for the averaged oxidation state $R32 Na_4V_2(PO_4)_3$). On the other hand, $K_4V_2(PO_4)_3$ retained a small band gap in all studied configurations. These results might provide valuable guidance for crystallography and electronic structure investigations for this important class of materials.

Keywords: density functional theory; hybrid-exchange-correlation functionals; NASICON; sodium vanadium phosphate



Citation: Gryaznov, D.; Vilčiauskas, L. On the Symmetry, Electronic Properties, and Possible Metallic States in NASICON-Structured $A_4V_2(PO_4)_3$ (A = Li, Na, K) Phosphates. *Materials* **2023**, *16*, 4361. <https://doi.org/10.3390/ma16124361>

Academic Editor: Marek Sierka

Received: 4 May 2023

Revised: 9 June 2023

Accepted: 11 June 2023

Published: 13 June 2023



Copyright: © 2023 by the authors. Licensee MDPI, Basel, Switzerland. This article is an open access article distributed under the terms and conditions of the Creative Commons Attribution (CC BY) license (<https://creativecommons.org/licenses/by/4.0/>).

1. Introduction

The ongoing search for new ion insertion materials with superior characteristics is one of the central themes in materials and electrochemical science [1]. They are at the heart of active electrode materials in batteries, desalination cells, and many other electrochemical devices. Na Superionic Conductor (NASICON) structure type phosphate frameworks with a general formula of $A_xM_2(PO_4)_3$ (where x is from 1 to 4, A is typically an alkali metal such as Li, Na, and K, and M is a transition metal, e.g., Ti, V, Cr, Fe, Mn, Co, Ni etc., or their combinations) are attracting a lot of attention [2–4]. This is due to their structural diversity, wide range of available redox potentials, electrochemical stability and reversibility, and high ionic mobility. These properties are useful not only for alternative battery technologies, but also for other electrochemical applications such as Faradaic deionization/desalination cells [5–10].

Further progress in this field still requires a lot of fundamental understanding as well as materials engineering in order to fully realize the potential of such framework materials. Despite a substantial theoretical effort, there is still a very limited understanding of the electronic structure and chemical bonding in these systems at an atomic level. In fact, it is these effects that really govern the material properties and behavior during electrochemical operation. These include the formation and mobility of ionic and polaronic charge carriers, interactions and ordering within the alkali, or transition metal sublattices, variation in the electronic band structure during ion insertion process etc. [11–15].

The analysis presented in this work was inspired by some of our recent results and the work of Wang et al. [16]. These results are based on Density Functional Theory (DFT) calculations of a fully sodiated $Na_4V_2(PO_4)_3$ composition and indicate the intriguing

possibility of an appearance of a metallic state in this particular phase. It is important to mention that NASICON-structured materials similar to other polyanionic framework compounds are typically assumed to be wide band gap semiconductors with a very low electronic charge carrier concentration and conductivity. In practice, there is a lot of additional processing and additives necessary when using these materials as electrodes. The potential existence of an unexpected metallicity in this class of materials could not just open new possibilities, but also would be very important to understand from a fundamental point of view.

The NASICON structure consists of an open framework of corner-sharing VO_6 octahedra and PO_4 tetrahedra with two different sites available for alkali metal occupation. At ambient conditions, NASICON compounds are typically assumed to adopt a high symmetry rhombohedral structure with a $R\bar{3}c$ (No. 167) space group (SG) (γ -phase). This is naturally expected in $\text{Na}_1\text{M}_2(\text{PO}_4)_3$ and $\text{Na}_4\text{M}_2(\text{PO}_4)_3$ structures, which both have fully occupied $M1$ or $\text{Na}1$ sites and either empty or fully occupied $M2$ or $\text{Na}2$ sites in the NASICON structure, respectively. Although recently, the second-order Jahn–Teller effect has been shown to exist and lead to the transition to a $R\bar{3}$ space group in NASICON systems with $x = 1$ [17]. However, for the intermediate occupation of $M2$ positions in $\text{Na}_2\text{M}_2(\text{PO}_4)_3$ and $\text{Na}_3\text{M}_2(\text{PO}_4)_3$ compositions, the situation is more complex. For example, $\text{Na}_3\text{V}_2(\text{PO}_4)_3$, due to Na disorder, adopts a $R\bar{3}c$ space group only above 177.2 °C [12], but, at lower temperatures sodium ordering and symmetry reduction is frequently observed [11,12,15,16].

The primitive unit cell of a fully occupied $\text{Na}_4\text{M}_2(\text{PO}_4)_3$ consists of 42 atoms ($Z = 2$): 8 Na, 4 M, 6 P, and 24 O atoms. Therefore, Na atoms are distributed among 2 $M1$ or $\text{Na}1$ (Wyckoff position: $6b$ (0, 0, 0)) and 6 $M2$ or $\text{Na}2$ (Wyckoff position: $18e$ ($x, 0, \frac{1}{4}$)) positions in the primitive unit cell. The position multiplicity in the conventional unit cell contains a three times larger number of atoms, i.e., $Z = 6$. In addition, oxygen ions occupy two low symmetry Wyckoff positions $36f$ with different coordinates, whereas vanadium ions occupy the Wyckoff position $12c$.

The local symmetry of a transition metal site also introduces another degree of freedom in terms of possible symmetries and sublattice ordering (also known as the Verwey-type ordering) in a NASICON structure. Even with only one type of metal is occupying the site, it might adopt a mixed-valence (or mixed-oxidation state) state due to charge neutrality requirements or disproportionation [13,18]. Throughout this work, the following nomenclature will be used for referring to the oxidation states (OSs) of vanadium in $\text{A}_4\text{V}_2(\text{PO}_4)_3$. The state of all vanadium atoms adopting equal fractional valence oxidation state of $\text{V}^{+2.5}$ will be interchangeably referred as averaged oxidation (valence), or non-mixed-valence state. The case where half of the vanadium atoms have V^{+2} and the other half V^{+3} oxidation states will be referred to as mixed-oxidation or mixed-valence state, interchangeably.

The symmetry and orderings in the alkali and transition metal sublattices are strongly dependent on the particular metal composition. Moreover, the experimental investigation of these effects is highly non-trivial, because high-intensity X-ray sources and a careful control of the sample preparation and measurement conditions are necessary [11].

In this study, we presented a comprehensive electronic structure analysis of NASICON-structured $\text{A}_4\text{V}_2(\text{PO}_4)_3$ systems, where $\text{A} = \text{Li}, \text{Na}, \text{K}$. We used high-level hybrid density functional theory calculations, the group theoretical symmetry approach, and the projected density of states analyses in this work. The structures with different alkali metals in the NASICON structure were fully optimized and analyzed in terms of available symmetries and band structure. A comparative analysis in terms of different-sized alkali metal cations by correspondingly replacing sodium with lithium and potassium was also performed. To the best of our knowledge, this is one of the first of such studies where the electronic aspects have been addressed in this class of materials at this level of detail and complexity.

2. Computational Methodology

Density Functional Theory (DFT) within Linear Combination of Atomic Orbitals (LCAO) formalism, together with B1WC hybrid-exchange-correlation functionals as imple-

mented in the CRYSTAL17 computer program, were used in this work [19,20]. All-Electron Gaussian basis sets of Triple-Zeta Valence with Polarization (TZVP) functions on Na, P and O were taken from Peintinger et al. [21]. In contrast, revised versions of pob-TZVP basis sets for Li, K, and V were taken from Vilela-Oliveira et al. [22]. The number of contracted basis functions (s/p/d/f) was 73211/511/1 for Na, 62111 for Li, 842111/6311/1 for K, 842111/6311/411/1 for V, 73211/5111/1 for P, and 6211/411/1 for O. The Monkhorst–Pack scheme was applied to select the k points on a 8x8x8 mesh for the integration of the first Brillouin zone in spin-polarized calculations of primitive unit cells [23]. The Coulomb and exchange integral tolerance factors of 8, 8, 8, and 16 were used in the calculations, together with an extra large numerical integration grid. The energy convergence threshold was set to 10^{-8} a.u. for the Self-Consistent Field (SCF) of total energy and 10^{-7} a.u. for the optimization of lattice parameters and atomic positions. We stress the importance of selecting an appropriate hybrid-exchange-correlation functional for the approximate treatment of electronic correlation effects in transition metal compounds [24]. It is well-known that standard Generalized-Gradient Approximation (GGA) exchange-correlation functionals underestimate the band gap and are unable to reproduce the correct electronic configuration, together with the associated structural distortions in transition metal compounds [24,25]. Hybrid-exchange-correlation functionals effectively combine Hartree–Fock (HF) and DFT approaches, which yield significantly better results and more accurate properties [24]. Wu and Cohen proposed a non-empirical exchange-correlation functional with an improved exchange part of the standard PBE density functional (denoted as WC functional) [26]. Bilk et al. [25] combined WC functional with hybrid B1 functional and a 0.16 mixing parameter for the exact exchange into B1WC hybrid-exchange-correlation functional. All the calculations were spin-polarized while assuming high spin states for V^{+2} [$3d^3$] and V^{+3} [$3d^2$]. The effective atomic charges and magnetic moments were calculated from the Mulliken population analysis.

3. Results and Discussion

3.1. Group Theoretical Approach to NASICON Structures

In the present study, we relied on crystallographic group theory and group-subgroup relations in order to construct low symmetry structures of $A_4V_2(PO_4)_3$ as well as to describe changes in the electronic structure appearing upon symmetry reduction. It is worth mentioning that such an approach is necessary, but not sufficient, to infer possible phase transitions. We also did not attempt to find the lowest possible symmetry, but mostly focused on the relationship between symmetry and total energy. The maximal subgroup approach provided a list of maximal subgroups for $R\bar{3}c$, which included $C2/c$, $R32$, $R\bar{3}$, $R3c$, and $P\bar{3}c1$ [27]. For simplicity, we limited ourselves to the monoclinic $C2$ SG and chose one chain of transitions. In this way, we suggest that considering only $C2$ SG is sufficient for discussing potential phase transitions to low symmetry phases in the present system. Among the maximal subgroups of $R\bar{3}c$, there were only two SGs: $R32$ and $C2/c$, which were both leading to $C2$. Moreover, the group-maximal subgroup tree (similar to the Bärnighausen tree) contained only two simple chains from $R\bar{3}c$ to $C2$, i.e., $R\bar{3}c \rightarrow C2/c \rightarrow C2$ and $R\bar{3}c \rightarrow R32 \rightarrow C2$ [28]. Moreover, the analysis of isotropy subgroups revealed that the $R\bar{3}c \rightarrow R32$ transition was determined by irreducible representation Γ_1^- , whereas the $R32 \rightarrow C2$ transition took place according to the primary irreducible representation Γ_3^- (Figure 1). In this work, the chain through $R32$ was chosen and used in the following procedure. At first, the system was relaxed in a high symmetry $R\bar{3}c$ supergroup; then, necessary symmetry operations were removed in order to relax the system in a lower symmetry rhombohedral structure (subgroup $R32$); finally, the necessary symmetry operations were removed from a relaxed lower symmetry rhombohedral structure (supergroup $R32$) in order to relax to the system in a low symmetry monoclinic structure (subgroup $C2$).

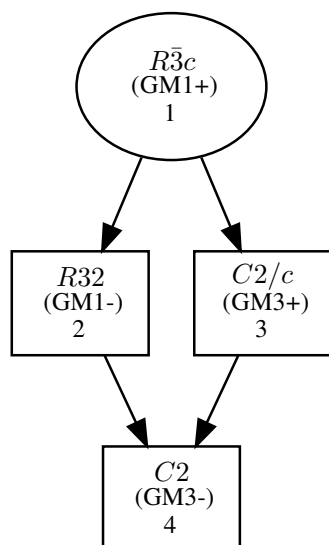


Figure 1. Graph of isotropy subgroups relating $R\bar{3}c$ and $C2$ [29].

3.2. Analysis of the Low Energy Structures

Having constructed structures with different symmetries, we proceeded to calculate and rank their energies in order to identify the ones with the lowest energies. At this point, it is worth noting that mixed OS cannot be obtained in a high symmetry $R\bar{3}c$ SG. $R32$ is the highest possible symmetry where mixed OS can be obtained in $A_4V_2(PO_4)_3$. In this case, two vanadium Wyckoff positions, which were of the same symmetry in $R\bar{3}c$ SG, split under symmetry reduction into two different Wyckoff 6c positions in the $R32$ SG.

The total energies of the structures with different SGs and OSs are compared with respect to the lowest energy structure (ground state) in Table 1. The ground state configuration for $Li_4V_2(PO_4)_3$ and $Na_4V_2(PO_4)_3$ adopted monoclinic symmetry with a $C2$ SG and an averaged vanadium OS ($V^{+2.5}$). This was different from the case of $K_4Ti_2(PO_4)_3$, which adopted mixed OSs (V^{+2}/V^{+3}), with $C2$ as the lowest energy structure. This indicates the importance of alkali metal on the structural and, as it is shown later, on the electronic properties of such compounds [13]. The relative energy differences between the lowest and higher energy structures were comparable for $Li_4V_2(PO_4)_3$ and $Na_4V_2(PO_4)_3$. The structures in the $R\bar{3}c$ SG and the averaged $V^{+2.5}$ OS were 0.597 eV/cell and 0.595 eV/cell higher in energy for $Li_4V_2(PO_4)_3$ and $Na_4V_2(PO_4)_3$, respectively. The $R32$ structures and mixed V^{+2}/V^{+3} OSs were 0.94 eV/cell and 0.825 eV/cell less favorable than the averaged OS $C2$ ones for $Li_4V_2(PO_4)_3$ and $Na_4V_2(PO_4)_3$, respectively. Also, the $R32$ structure with the averaged OS was the second lowest energy structure in both $Na_4V_2(PO_4)_3$ and $Li_4V_2(PO_4)_3$. The important finding here is that, identically to the previous results of Wang et al. [16] using the SCAN+U approach, the B1WC hybrid functional also showed that $Li_4V_2(PO_4)_3$ and $Na_4V_2(PO_4)_3$ structures with averaged OSs were lower in energy than those with a mixed valence. The hypothetical phase transition from $R\bar{3}c$ to $R32$ would correspond to the charge ordering transition within the mixed oxidation V^{+2}/V^{+3} sublattice without any accompanying A^+ -vacancy ordering due to full alkali metal sublattice occupancy.

In contrast to Na- and Li- based $A_4V_2(PO_4)_3$ NASICON structures, the $C2$ SG and mixed V^{+2}/V^{+3} OS had the lowest energy in $K_4V_2(PO_4)_3$ (Table 1). This suggests that symmetry reduction down to monoclinic symmetry was favorable in all three studied systems. Moreover, the energy differences between different symmetry configurations were a bit smaller in $K_4V_2(PO_4)_3$ than in the other two cases. $K_4V_2(PO_4)_3$ with the $C2$ SG and averaged $V^{+2.5}$ OS was only 0.200 eV/cell, and with $R\bar{3}c$, its averaged OS was only 0.153 eV/cell less stable than the ground state structure.

The results suggest that it is not only the overall symmetry reduction and the type of vanadium OS that have an effect on the structure and stability of these compounds.

The ionic size, and potentially the electronic structure of the ion at the alkali metal site, also seem to play an important role.

Table 1. The structural properties of $A_4V_2(PO_4)_3$ as calculated with the B1WC hybrid functional. a, c lattice parameters in the hexagonal setting, q effective atomic charge of vanadium from Mulliken analysis, μ magnetic moment of vanadium atoms, band gap value E_g , and total energy difference with respect to the ground state structure are marked in bold. The results for $Na_4V_2(PO_4)_3$ and $Li_4V_2(PO_4)_3$ with the mixed OS in the C2 SG are not shown, as the energy difference with the $R32$ SG did not exceed 0.004 eV/cell and was insignificant. Analysis of free parameters in atomic positions is also excluded.

	$a/\text{\AA}$	$c/\text{\AA}$	q/e	μ/μ_B	E_g/eV	$\Delta E_{tot}/eV$ /cell
$R\bar{3}c$ / Average OS: $V^{+2.5}$						
$Li_4V_2(PO_4)_3$	8.96	19.58	+1.17	2.56	0	0.597
$Na_4V_2(PO_4)_3$	8.97	21.15	+1.19	2.57	0	0.595
$K_4V_2(PO_4)_3$	9.20	22.33	+1.21	2.55	0.35	0.224
$R32$ / Average OS: $V^{+2.5}$						
$Li_4V_2(PO_4)_3$	8.97	19.49	$V^{+2.5}$ +1.18 $V^{+2.5}$ +1.17	$V^{+2.5}$ 2.53 $V^{+2.5}$ 2.56	0	0.352
$Na_4V_2(PO_4)_3$	8.97	21.17	$V^{+2.5}$ +1.20 $V^{+2.5}$ +1.20	$V^{+2.5}$ 2.53 $V^{+2.5}$ 2.53	0.41	0.141
$K_4V_2(PO_4)_3$	9.20	22.33	$V^{+2.5}$ +1.21 $V^{+2.5}$ +1.21	$V^{+2.5}$ 2.55 $V^{+2.5}$ 2.55	0.35	0.224
$R32$ / Mixed OS: V^{+2}/V^{+3}						
$Li_4V_2(PO_4)_3$	8.97	19.58	V^{+2} +1.10 V^{+3} +1.20	V^{+2} 2.99 V^{+3} 2.11	0	0.940
$Na_4V_2(PO_4)_3$	8.98	21.15	V^{+2} +1.14 V^{+3} +1.18	V^{+2} 3.00 V^{+3} 2.11	0	0.825
$K_4V_2(PO_4)_3$	9.22	22.38	V^{+2} +1.15 V^{+3} +1.23	V^{+2} 3.00 V^{+3} 2.04	0.55	0.153
$C2$ / Average OS: $V^{+2.5}$						
$Li_4V_2(PO_4)_3$	8.96 $b = 9.96$	19.60	+1.18	2.55	0.20	0
$Na_4V_2(PO_4)_3$	8.96 $b = 9.97$	21.18	+1.19	2.55	0.13	0
$K_4V_2(PO_4)_3$	9.24 $b = 9.20$	22.31	+1.20	2.56	0.17	0.200
$C2$ / Mixed OS: V^{+2}/V^{+3}						
$K_4V_2(PO_4)_3$	9.21	22.34	V^{+2} +1.15 V^{+3} +1.22	V^{+2} 3.00 V^{+3} 2.07	0.76	0

3.3. Electronic Structure Analysis

The electronic structure and properties of the $A_4V_2(PO_4)_3$ system are the main focus of the present study. Table 1 summarizes the calculated Mulliken effective atomic charges (q) and magnetic moments (μ) for vanadium ions in all studied structures. As expected, the charge values were correlated with the formal OS. There was also a clear correlation between the V charge in structures with different alkali metals: Li compounds always showed lower charges, followed by Na, and then by K. $Na_4V_2(PO_4)_3$ and $Li_4V_2(PO_4)_3$ systems adopted averaged OSs and C2 SGs in the ground state and showed small band gaps of 0.13 eV and 0.20 eV, respectively (Table 1). $K_4V_2(PO_4)_3$ in the ground state, identically to $Na_4Ti_2(PO_4)_3$ [13], adopted a mixed OS but featured an C2 SG with a band gap of 0.76 eV. The most interesting feature of this study is that any studied symmetry increase in $Li_4V_2(PO_4)_3$ either to the SG $R32$ or $R\bar{3}c$ showed a closing of the band gap. However,

$\text{Na}_4\text{V}_2(\text{PO}_4)_3$ demonstrated the presence of a non-zero band gap for the averaged OS in the $R32$ SG and a zero band gap for averaged OS in the $R\bar{3}c$ SG. In contrast to $\text{Na}_4\text{V}_2(\text{PO}_4)_3$ and $\text{Li}_4\text{V}_2(\text{PO}_4)_3$, $\text{K}_4\text{V}_2(\text{PO}_4)_3$ had a finite band gap in all studied symmetry configurations and vanadium OSs (Table 1). Hereafter, we refer to systems with zero band gaps as metallic.

The calculated DOSs for the $\text{A}_4\text{V}_2(\text{PO}_4)_3$ systems are presented in Figure 2. In the following, we only compared the following cases, namely, those with high symmetry $R\bar{3}c$ SGs and averaged $\text{V}^{+2.5}$ OSs, mixed $\text{V}^{+2}/\text{V}^{+3}$ OSs in an $R32$ SG (Figure 2), and averaged OSs in a monoclinic $C2$ SG. One can see that bands close to the Fermi level in all $\text{A}_4\text{V}_2(\text{PO}_4)_3$ systems were formed by V 3d-states. Crystal Orbital Overlap Population (COOP) analysis was also performed in order to analyze the bonding character of these states. Identically to our previous results on $\text{Na}_2\text{VTi}(\text{PO}_4)_3$, COOP analysis showed the states close to the Fermi level to have mostly anti-bonding character in all studied $\text{A}_4\text{V}_2(\text{PO}_4)_3$ systems as well [30]. The band gap, if present, was of a d-d character and appeared due to a separate band formed by empty V 3d-states in the spin-up channel (Figure 2, top-left).

This band shifted to lower energies and crossed the Fermi level in $\text{Li}_4\text{V}_2(\text{PO}_4)_3$ and $\text{Na}_4\text{V}_2(\text{PO}_4)_3$ for the mixed vanadium OSs in the high symmetry $R32$ structures (Figure 2, top-right). In contrast, the separate empty band remained in $\text{K}_4\text{V}_2(\text{PO}_4)_3$ which showed a finite band gap remaining in all configurations such as the averaged OS $C2$ (0.17 eV), mixed OS $R32$ (0.55 eV), and averaged OS $R\bar{3}c$ (0.35 eV). Notice that the DOS for the ground state of $\text{K}_4\text{V}_2(\text{PO}_4)_3$ with the mixed OS in the $C2$ SG is not shown. We found its DOS to be identical to the one of the $R32$ SG.

In Figure 2, one can see that, in the case of a mixed OS $\text{K}_4\text{V}_2(\text{PO}_4)_3$ system, the empty conduction band was formed by V^{+3} states right above the Fermi energy at 0.55 eV. In contrast, neither $\text{Li}_4\text{V}_2(\text{PO}_4)_3$ nor $\text{Na}_4\text{V}_2(\text{PO}_4)_3$ demonstrated the presence of a separate empty band above the Fermi energy and remained metallic in the mixed OS configurations. However, the reduction of symmetry down to the monoclinic $C2$ structure led to the appearance of an empty band, as well as the formation of a small gap in the latter two systems. Although the closing of band gap and the appearance of a metallic state are commonly attributed to a stronger delocalization of 3d electrons, our results showed it was only partially valid in these compounds. Our results also showed that Li- and Na-based systems showed almost identical electronic structures in Figure 2. Neither the ionic size nor the electronic configuration such as the presence of p-electrons seemed to have any significant effect on the band structure or the appearance of metallicity in $\text{Li}_4\text{V}_2(\text{PO}_4)_3$ and $\text{Na}_4\text{V}_2(\text{PO}_4)_3$. Only the introduction of larger K ions destroyed the metallic state in $\text{A}_4\text{V}_2(\text{PO}_4)_3$ and resulted in marked structural changes.

The calculated DOSs could at least partially explain why the average OS was preferred over the mixed OS in $\text{Na}_4\text{V}_2(\text{PO}_4)_3$ and $\text{Li}_4\text{V}_2(\text{PO}_4)_3$. It is due to occupied V^{+3} states intermixing with occupied V^{+2} states in the energy range between -1 eV and the Fermi energy, which is energetically preferred (Figure 2 (top right)). Even though $\text{Na}_4\text{V}_2(\text{PO}_4)_3$ demonstrates the non-zero band gap for the averaged OS in the $R32$ SG, the intermixing of states is still an important property. On the contrary, $\text{K}_4\text{V}_2(\text{PO}_4)_3$ did not demonstrate the same intermixing because occupied V^{+2} and V^{+3} bands were well separated in this structure.

Another interesting observation of this work was the analysis of a parent $\text{Na}_3\text{V}_2(\text{PO}_4)_3$ composition. The typical structure has all $M1$ (1/4 of total) sodium sites occupied, and these sodium atoms are not (electro)chemically exchangeable. The remaining 2/4 of Na atoms are distributed over 3 $M2$ sites, with some ordering observed at low temperatures [12,15]. In this work, we constructed a hypothetical rhombohedral $\text{Na}_3\text{V}_2(\text{PO}_4)_3$ with an $R\bar{3}c$ SG. For this, we used pure symmetry considerations by removing Na atoms from $M1$ site (Wyckoff position $6b$) in $\text{Na}_4\text{V}_2(\text{PO}_4)_3$. In this way, rhombohedral symmetry was maintained, and all $M2$ positions were fully occupied. The DOS analysis in Figure 3 (top) shows that this particular configuration of $\text{Na}_3\text{V}_2(\text{PO}_4)_3$ with high $R\bar{3}c$ symmetry and an averaged $\text{V}^{+2.5}$ OS was also metallic. Moreover, its band electronic structure was almost identical to

that of $\text{Na}_4\text{V}_2(\text{PO}_4)_3$ in the same symmetry and OS structure. These results indicate that the full occupancy of $M2$ sites in $\text{Na}_3\text{V}_2(\text{PO}_4)_3$ tends to close the band gap.

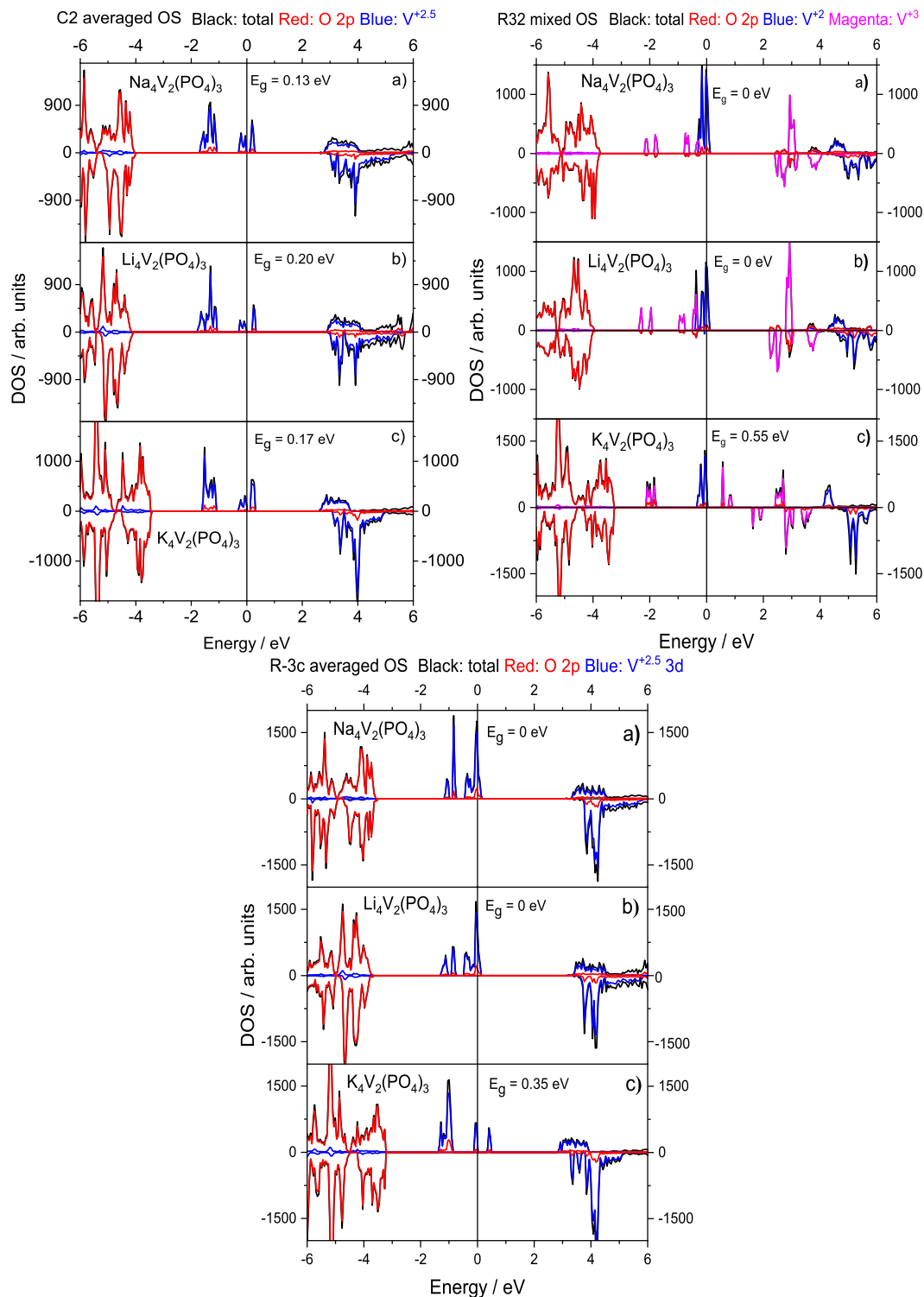


Figure 2. Total and atom projected DOS for (top left) C2 averaged $\text{V}^{+2.5}$ OS, (top right) R32 mixed $\text{V}^{+2}/\text{V}^{+3}$ OS, and (bottom) $\text{R}\bar{3}\text{c}$ averaged $\text{V}^{+2.5}$ OS in (a) $\text{Na}_4\text{V}_2(\text{PO}_4)_3$, (b) $\text{Li}_4\text{V}_2(\text{PO}_4)_3$, and (c) $\text{K}_4\text{V}_2(\text{PO}_4)_3$. Positive and negative DOS values denote the spin-up and spin-down states, respectively. Fermi energy is taken as 0.

The structure of the most important bands close to the Fermi energy could be also analyzed in terms of DOS projections on the symmetry-allowed irreducible representations

(Figure 3 (bottom)). In accordance with the local V site symmetry with point group C_3 in both $R32$ and $R\bar{3}c$ SGs of $A_4V_2(PO_4)_3$, the 3d orbitals split into a non-degenerate $A(d_{z^2})$ orbital in $R\bar{3}c$ ($A_1(d_{z^2})$ orbital in $R32$) and two two-fold degenerate $E(d_{xz}, d_{yz})$ and $E(d_{x^2-y^2}, d_{xy})$ orbitals. The A and E orbitals form separate bands which is reflected in the calculated DOS.

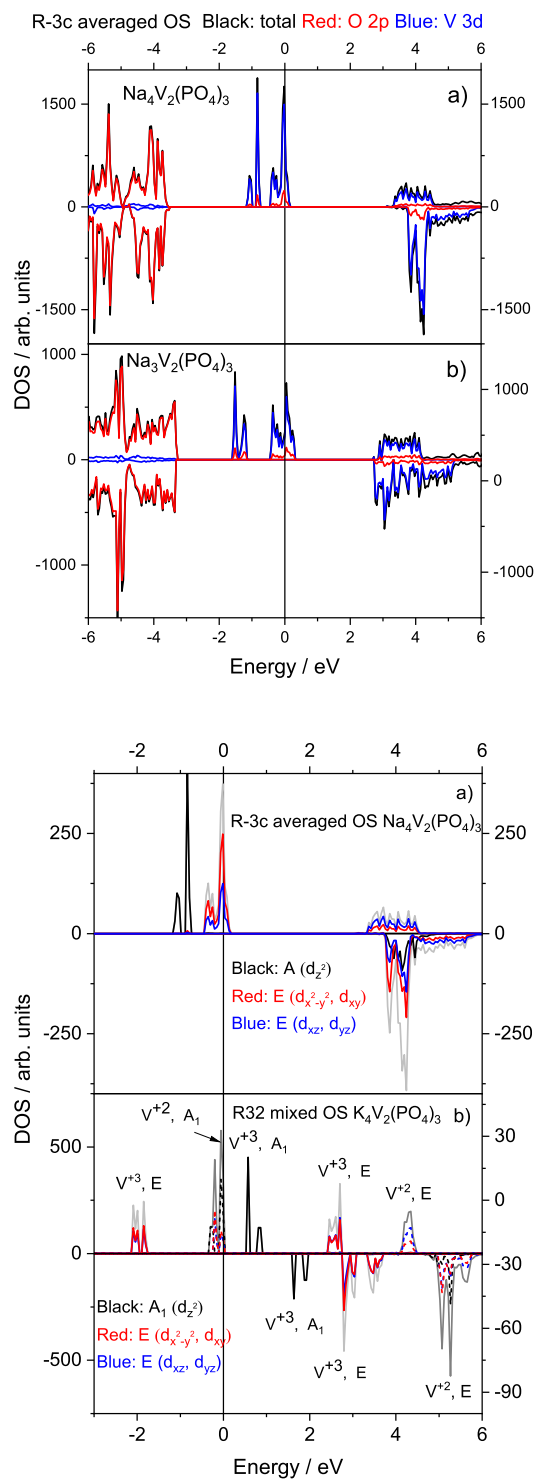


Figure 3. (top) Total and atom projected DOS for (a) $Na_4V_2(PO_4)_3$ and (b) $Na_3V_2(PO_4)_3$ with the averaged OS in the $R\bar{3}c$ SG. (bottom) Orbital DOS projections based on the symmetry-allowed irreducible representations for (a) $Na_4V_2(PO_4)_3$ with averaged OS and $R\bar{3}c$ SG, and (b) $K_4V_2(PO_4)_3$ with mixed OS and $R32$ SG. The Fermi energy is taken as 0. Dashed lines represent +2 states only.

For $\text{Na}_4\text{V}_2(\text{PO}_4)_3$ in the $R\bar{3}c$ SG, the two two-fold degenerate E orbitals comprise the band at the Fermi energy, and the empty states just above it (metallic state). Obviously, the occupation of E orbitals is possible not only due to symmetry properties but also due to delocalization effects as discussed above. As vanadium is octahedrally coordinated by oxygens in $[\text{VO}_6]$, the second band comprises only the non-degenerate A-orbital, which most likely interacts with the O $2p_z$ orbital (Figure 3). In the high symmetry $R\bar{3}c$ SG structure, the two-fold degenerate E orbitals interact with O $2p_x$ and $2p_y$ orbitals. Moreover, the bottom of the conduction band mostly comprises two two-fold degenerate E orbitals.

The structure of the orbital-projected DOS was quite different in the case of $\text{K}_4\text{V}_2(\text{PO}_4)_3$ with the mixed OS in the $R32$ SG. Only two important features are common for the average OS $R\bar{3}c$ of $\text{Na}_4\text{V}_2(\text{PO}_4)_3$ and $\text{K}_4\text{V}_2(\text{PO}_4)_3$: (i) in accordance with the rhombohedral symmetry, the two degenerate E orbitals are intermixed, and (ii) for the same symmetry reasons, the degenerate and non-degenerate orbitals are clearly separated. Obviously, some additional bands appear due to the separation of V^{+2} and V^{+3} 3d electrons in the mixed OS, thereby doubling the number of electronic bands. In the mixed OS $\text{K}_4\text{V}_2(\text{PO}_4)_3$ case, it is mostly the non-degenerate A_1 orbitals contributing to the top of the valence band. Moreover, this separation between the A_1 orbitals of V^{+2} and V^{+3} states leads to the opening of a 0.55 eV band gap in the $R32$ SG case (Figure 3). The occupied and unoccupied degenerate V^{+3} state E orbitals lay at ~ -1.8 eV and at 2.3–3.9 eV from the Fermi level, respectively. In contrast, the degenerate V^{+2} state E orbitals are unoccupied and lay above 4 eV from the Fermi level.

4. Conclusions

1. NASICON-structured $\text{Li}_4\text{V}_2(\text{PO}_4)_3$ and $\text{Na}_4\text{V}_2(\text{PO}_4)_3$ with fully occupied alkali metal sites adopt monoclinic structures with C2 SGs and averaged vanadium OS $\text{V}^{+2.5}$ in the ground state. On the other hand, $\text{K}_4\text{V}_2(\text{PO}_4)_3$ adopted a monoclinic structure with a C2 SG, which was stabilized by the mixed vanadium oxidation state $\text{V}^{+2}/\text{V}^{+3}$ in the ground state.
2. $\text{Li}_4\text{V}_2(\text{PO}_4)_3$ and $\text{Na}_4\text{V}_2(\text{PO}_4)_3$ possessed small band gaps of 0.13 eV and 0.20 eV in the ground state, respectively. However, monoclinic to rhombohedral symmetry increases closed the band gap and demonstrated the possibility of a metallic state in both the $\text{V}^{+2.5}$ averaged (in the $R\bar{3}c$ SG for $\text{Na}_4\text{V}_2(\text{PO}_4)_3$ and the $R\bar{3}c$ and $R32$ SGs for $\text{Li}_4\text{V}_2(\text{PO}_4)_3$) and $\text{V}^{+2}/\text{V}^{+3}$ mixed vanadium oxidation states. In contrast, $\text{K}_4\text{V}_2(\text{PO}_4)_3$ retained a small band gap in all studied structures with different symmetries and vanadium OSs.
3. The band gap in these structures was of a d-d character, independent of the symmetry or vanadium oxidation state. In the case of mixed vanadium oxidation, it was due to an empty band formed by the V^{+3} states.
4. The special configuration of high $R\bar{3}c$ symmetry $\text{Na}_3\text{V}_2(\text{PO}_4)_3$ with Na atoms removed from all M1 sites but completely occupied M2 sites as in initial $\text{Na}_4\text{V}_2(\text{PO}_4)_3$ also showed the appearance of a metallic state.
5. The orbital-projected DOS analysis for a rhombohedral symmetry shows that, in an averaged oxidation state for $\text{Na}_4\text{V}_2(\text{PO}_4)_3$, the band around the Fermi level is mostly comprised of two-fold degenerate E orbitals, whereas, in the mixed OS, it is mostly the non-degenerate A_1 orbitals contributing to the top of the valence band. Moreover, the separation between the A_1 orbitals of V^{+2} and V^{+3} states led to the opening of a band gap.
6. These results might contribute to a fundamental understanding of the crystal and electronic structure, as well as provide valuable guidance for researchers performing experimental investigations on this important class of materials.

Author Contributions: Conceptualization, D.G. and L.V.; methodology, D.G. and L.V.; software, D.G.; validation, D.G. and L.V.; formal analysis, D.G.; investigation, D.G. and L.V.; resources, D.G. and L.V.; data curation, D.G.; writing—original draft preparation, D.G. and L.V.; writing—review

and editing, D.G. and L.V.; visualization, D.G.; funding acquisition, D.G. and L.V. All authors have read and agreed to the published version of the manuscript.

Funding: This project has received funding from the European Regional Development Fund (Project No. 01.2.2-LMT-K-718-02-0005) under grant agreement with the Research Council of Lithuania (LMTLT). The Institute of Solid State Physics through the University of Latvia as the Center of Excellence has received funding from the European Union's Horizon 2020 Framework Programme H2020-WIDESPREAD-01-2016-2017-TeamingPhase2 under grant agreement No. 739508, project CAMART².

Data Availability Statement: The data presented in this study are available in the article.

Acknowledgments: The authors wish to thank Guntars Zvejnieks for discussions on group-theory analysis and for helping with the Bilbao Crystallographic Server.

Conflicts of Interest: The authors declare no conflict of interest. The funders had no role in the design of the study; in the collection, analyses, or interpretation of data; in the writing of the manuscript; or in the decision to publish the results.

Abbreviations

The following abbreviations are used in this manuscript:

DFT	Density Functional Theory
LCAO	Linear Combination of Atomic Orbitals
OS	Oxidation State
SG	Space Group
WC	Wu–Cohen
NVP	Na ₃ V ₂ (PO ₄) ₃

References

1. Yang, Z.; Zhang, J.; Kintner-Meyer, M.C.W.; Lu, X.; Choi, D.; Lemmon, J.P.; Liu, J. Electrochemical Energy Storage for Green Grid. *Chem. Rev.* **2011**, *111*, 3577–3613. [[CrossRef](#)]
2. Masquelier, C.; Croguennec, L. Polyanionic (Phosphates, Silicates, Sulfates) Frameworks as Electrode Materials for Rechargeable Li (or Na) Batteries. *Chem. Rev.* **2013**, *113*, 6552–6591. [[CrossRef](#)] [[PubMed](#)]
3. Jian, Z.; Hu, Y.S.; Ji, X.; Chen, W. NASICON-Structured Materials for Energy Storage. *Adv. Mater.* **2017**, *29*, 1601925. [[CrossRef](#)]
4. Chen, S.; Wu, C.; Shen, L.; Zhu, C.; Huang, Y.; Xi, K.; Maier, J.; Yu, Y. Challenges and Perspectives for NASICON-Type Electrode Materials for Advanced Sodium-Ion Batteries. *Adv. Mater.* **2017**, *29*, 1700431. [[CrossRef](#)]
5. Palomares, V.; Serras, P.; Villaluenga, I.; Hueso, K.B.; Carretero-Gonzalez, J.; Rojo, T. Na-ion batteries, recent advances and present challenges to become low cost energy storage systems. *Energy Environ. Sci.* **2012**, *5*, 5884–5901. [[CrossRef](#)]
6. Slater, M.D.; Kim, D.; Lee, E.; Johnson, C.S. Sodium-Ion Batteries. *Adv. Funct. Mater.* **2013**, *23*, 947–958. [[CrossRef](#)]
7. Kundu, D.; Talaie, E.; Duffort, V.; Nazar, L.F. The Emerging Chemistry of Sodium Ion Batteries for Electrochemical Energy Storage. *Angew. Chem.-Int. Edit.* **2015**, *54*, 3431–3448. [[CrossRef](#)]
8. Yabuuchi, N.; Kubota, K.; Dahbi, M.; Komaba, S. Research Development on Sodium-Ion Batteries. *Chem. Rev.* **2014**, *114*, 11636–11682. [[CrossRef](#)]
9. Nayak, P.K.; Yang, L.; Brehm, W.; Adelhalm, P. From Lithium-Ion to Sodium-Ion Batteries: Advantages, Challenges, and Surprises. *Angew. Chem.-Int. Edit.* **2018**, *57*, 102–120. [[CrossRef](#)] [[PubMed](#)]
10. Wang, L.; Zhang, Y.; Moh, K.; Presser, V. From capacitive deionization to desalination batteries and desalination fuel cells. *Curr. Opin. Electrochem.* **2021**, *29*, 100758. [[CrossRef](#)]
11. Kabbour, H.; Coillot, D.; Colmont, M.; Masquelier, C.; Mentre, O. α -Na₃M₂(PO₄)₃ (M = Ti, Fe): Absolute Cationic Ordering in NASICON-Type Phases. *J. Am. Chem. Soc.* **2011**, *133*, 11900–11903. [[CrossRef](#)] [[PubMed](#)]
12. Chotard, J.N.; Rouse, G.; David, R.; Mentré, O.; Courty, M.; Masquelier, C. Discovery of a Sodium-Ordered Form of Na₃V₂(PO₄)₃ below Ambient Temperature. *Chem. Mater.* **2015**, *27*, 5982–5987. [[CrossRef](#)]
13. Gryaznov, D.; Stauffer, S.K.; Kotomin, E.A.; Vilčiauskas, L. Hybrid density functional theoretical study of NASICON-type Na_xTi₂(PO₄)₃ (x = 1–4). *Phys. Chem. Chem. Phys.* **2020**, *22*, 11861–11870. [[CrossRef](#)]
14. Snarskis, G.; Pilipavičius, J.; Gryaznov, D.; Mikoliunaitė, L.; Vilčiauskas, L. Peculiarities of Phase Formation in Mn-Based Na Superionic Conductor (NaSiCon) Systems: The Case of Na_{1+2x}Mn_xTi_{2-x}(PO₄)₃ (0.0 ≤ x ≤ 1.5). *Chem. Mater.* **2021**, *33*, 8394–8403. [[CrossRef](#)]
15. Park, S.; Wang, Z.; Deng, Z.; Moog, I.; Canepa, P.; Fauth, F.; Carlier, D.; Croguennec, L.; Masquelier, C.; Chotard, J.N. Crystal Structure of Na₂V₂(PO₄)₃, an Intriguing Phase Spotted in the Na₃V₂(PO₄)₃–Na₁V₂(PO₄)₃ System. *Chem. Mater.* **2021**, *34*, 451–462. [[CrossRef](#)]

16. Wang, Z.; Park, S.; Deng, Z.; Carlier, D.; Chotard, J.N.; Croguennec, L.; Gautam, G.S.; Cheetham, A.K.; Masquelier, C.; Canepa, P. Phase stability and sodium-vacancy orderings in a NaSICON electrode. *J. Mater. Chem. A* **2022**, *10*, 209–217. [[CrossRef](#)]
17. Nagai, T.; Mochizuki, Y.; Yoshida, S.; Kimura, T. Chemical Aspect of Displacive-Type Ferroaxial Phase Transition from Perspective of Second-Order Jahn–Teller Effect: NASICON Systems as an Example. *J. Am. Chem. Soc.* **2023**, *145*, 8090–8098. [[CrossRef](#)]
18. Yin, S.; Grondy, H.; Strobel, P.; Huang, H.; Nazar, L. Charge ordering in lithium vanadium phosphates: Electrode materials for lithium-ion batteries. *J. Am. Chem. Soc.* **2003**, *125*, 326–327. [[CrossRef](#)]
19. Dovesi, R.; Saunders, V.; Roetti, C.; Orlando, R.; Zicovich-Wilson, C.; Pascale, F.; Civalleri, B.; Doll, K.; Harrison, N.; Bush, I.; et al. *CRYSTAL17 User's Manual*; University of Torino: Torino, Italy, 2017.
20. Dovesi, R.; Erba, A.; Orlando, R.; Zicovich-Wilson, C.M.; Civalleri, B.; Maschio, L.; Rérat, M.; Casassa, S.; Baima, J.; Salustro, S.; et al. Quantum-mechanical condensed matter simulations with CRYSTAL. *WIRE Comput. Mol. Sci.* **2018**, *8*, e1360. [[CrossRef](#)]
21. Peintinger, M.F.; Oliveira, D.V.; Bredow, T. Consistent gaussian basis sets of Triple-Zeta valence with polarization quality for solid-State Calculations. *J. Comput. Chem.* **2013**, *34*, 451–459. [[CrossRef](#)] [[PubMed](#)]
22. Vilela Oliveira, D.; Laun, J.; Peintinger, M.F.; Bredow, T. BSSE-correction scheme for consistent gaussian basis sets of double- and triple-zeta valence with polarization quality for solid-state calculations. *J. Comput. Chem.* **2019**, *40*, 2364–2376. [[CrossRef](#)]
23. Monkhorst, H.J.; Pack, J.D. Special points for Brillouin-zone integrations. *Phys. Rev. B* **1976**, *13*, 5188–5192. [[CrossRef](#)]
24. Franchini, C. Hybrid functionals applied to perovskites. *J. Phys.-Condes. Matter.* **2014**, *26*, 253202. [[CrossRef](#)] [[PubMed](#)]
25. Bilk, D.I.; Orlando, R.; Shaltaf, R.; Rignanese, G.M.; Iniguez, J.; Ghosez, P. Hybrid exchange-correlation functional for accurate prediction of the electronic and structural properties of ferroelectric oxides. *Phys. Rev. B* **2008**, *77*, 165107. [[CrossRef](#)]
26. Wu, Z.; Cohen, R.E. More accurate generalized gradient approximation for solids. *Phys. Rev. B* **2006**, *73*, 235116. [[CrossRef](#)]
27. Aroyo, M.I.; Perez-Mato, J.M.; Capillas, C.; Kroumova, E.; Ivantchev, S.; Madariaga, G.; Kirov, A.; Wondratschek, H. Bilbao Crystallographic Server: I. Databases and crystallographic computing programs. *Z. Für Krist.-Cryst. Mater.* **2006**, *221*, 15–27. [[CrossRef](#)]
28. Ivantchev, S.; Kroumova, E.; Madariaga, G.; Pérez-Mato, J.M.; Aroyo, M.I. *SUBGROUPGRAPH*: A Comput. Program Anal. Group- Relations Space Groups. *J. Appl. Crystallogr.* **2000**, *33*, 1190–1191. [[CrossRef](#)]
29. Bilbao Crystallographic Server. 2023. Available online: <https://www.cryst.ehu.es/> (accessed on 20 April 2023).
30. Petrulėvičienė, M.; Pilipavičius, J.; Juodkazytė, J.; Gryaznov, D.; Vilčiauskas, L. Electrochemical Performance of NASICON-structured $\text{Na}_{3-x}\text{V}_{2-x}\text{Ti}_x(\text{PO}_4)_3$ ($0.0 < x < 1.0$) as aqueous Na-ion battery positive electrodes. *Electrochim. Acta* **2022**, *424*, 140580.

Disclaimer/Publisher's Note: The statements, opinions and data contained in all publications are solely those of the individual author(s) and contributor(s) and not of MDPI and/or the editor(s). MDPI and/or the editor(s) disclaim responsibility for any injury to people or property resulting from any ideas, methods, instructions or products referred to in the content.